RESEARCH ARTICLE

Spectrometric measurement of human teeth plasma produced by nanosecond Nd:YAG pulsed laser

Suhad S. Dakhil[1] · Tagreed K. Hamad[1]

Abstract Spectroscopic measurements of human teeth plasma parameters are carried out utilizing the fundamental and second harmonics (1064 and 532 nm) of Nd:YAG laser. The laser irradiance ranging from 1.9 to 9.9×10^9 W/cm^2 was directed on the sample in order to produce plasma. Calcium emission lines have been investigated and utilized to compute the plasma parameters based on experimental findings. We identified laser-induced plasma characteristics such as electron temperature (T_e) using the Boltzmann and the density of electron (N_e) using the two-line ratio method. T_e and N_e values increased as laser energy increased. The estimated range of Te was (10549–24683)K for 1064 nm and (10179–21896)K for 532nm while the range of Ne was $(1.26* 1016–6.87*1016)$ cm^{-3} for 1064 nm $(2.2*1016–9.8*1016)cm^{-3}$ for 532 nm. The variation of other plasma parameter such as Debye length (λ_D/cm), particles number in Debye sphere (N_D/cm^3), and plasma frequency (ω_p/Hz) with laser irradiance have also been investigated.

Keywords Human teeth · Laser-induced plasma · Spectrometric measurement · Ca emission lines

Introduction

The widely-used spectroscopic analysis method named as laser-induced breakdown spectroscopy (LIBS) involves the use of a high-powered laser beam directed at the surface of a target material [1–3]. This laser beam vaporizes, excites, and ionizes the target species, causing the emission of light when the species de-excite or recombine [4]. This emitted light is collected and subjected to spectral analysis to extract valuable information such as elemental identification, quantification, and plasma parameters [5, 6]. The behavior of the plasma is influenced by a range of laser parameters, including incident energy, wavelength, and pulse duration, as well as target material properties [7]. The species appear in the plasma can interact with the incident photons, leading to further heating of the plume, and finally, radiation is emitted from the expanded plasma for an extended duration. By examining the emissions from excited species, it becomes possible to identify the elemental composition of the plasma as it approximately represents the analyte's content [8, 9]. In recent decades, the technique of LIBS has gained recognition as a reliable analytical method across various fields of application. One of its notable advantages is its non-contact, optical nature, which eliminates the need for sample preparation [10]. Numerous areas of application have already been established, such as elemental analysis [11], quality control in steel manufacturing, and characterization of jewelry products [12]. Additionally, LIBS has been utilized in soil studies, thin film deposition, cleaning, preservation of cultural heritage [13] (e.g., cleaning of old papers, wood, and paintings), as well as *in situ* planetary exploration. Despite the utilization of the LIBS to examine elemental composition of biological samples, limited studies exist on the use of LIBS for investigating plasma produced at human tooth surface. Hence, the present study aimed to look at the correlation between plasma parameters, photon absorption, and laser wavelength, as this information is pivotal in controlling the plasma. Some other plasma parameters (Debye length,

✉ Tagreed K. Hamad
tagreed_k@yahoo.com

Suhad S. Dakhil
suhad_@gmail.com

1 Laser and Optoelectronics Department, College of Engineering, Al-Nahrain University, Baghdad, Iraq

number of particles in Debye sphere, and plasma frequency) were considered as well.

Materials and methods

In this experiment, tooth samples are randomly chosen from the Al-Kut Specialized Dental Center in Wasit Governorate, Iraq. All samples were obtained after informed consent of the patients and doctor. These samples are washed in distilled water and stored in numbered sealed pots. Figure 1 depicts a typical LIBS analysis system used to produced plasma, it mainly consists of laser source, collection optics, analysis device, and material target. The information of a laboratory-made arrangement are introduced in Table 1.

Results and discussion

Plasma emission and identification of elements

Emission spectra of laser-produced tooth plasma captured at spectral window of 250–650 nm are shown in Fig. 2 for two different wavelengths (1064 and 532 nm). Beside continuum background, predominated ionic and atomic emission lines have been assigned. The significant major, minor, and trace element observed in the samples were Ca, P, Mg, Si, Sr, Ti, and Cr.

According to the NIST database [14], a number of characteristic emission lines for Ca were found in the plasma spectrum. Among of many detected lines, Ca II 396.84 nm and Ca II 422.67 nm will be utilized to both compute plasma parameters (N_e and T_e) and to study the plasma dependence on laser irradiance. Figure 3 displays the variation in the intensity of the calcium lines with laser irradiance. As a result of increasing laser ablation rate, the plasma's ability to absorb laser light increases with increased laser irradiation leading to an increase in spectral line intensity. However, one can see an increase in the line emission intensity for both spectral lines Ca II 396.84 and Ca II 422.67 nm with laser wavelength 1064 nm compared to 532 nm at fixed laser energy. Same trend has been concluded by other researchers [15–17]. This was explained by the distinctions between optical and thermal characteristics of calcium element in visible (Vis.) and infrared (IR.) laser spectral regions.

Variation of plasma temperature (Te)

Plasma temperature and electron number density are two essential parameters for realizing excitation and ionization

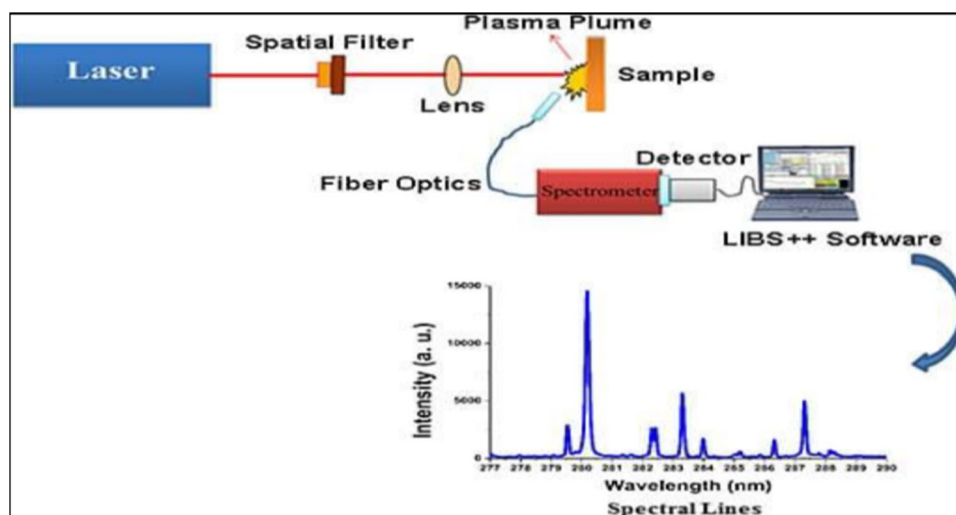**Fig. 1** Schematic diagram of LIBS setup

Table 1 Setup details for samples analysis

Nd:YAG laser	Wavelengths (532 and 1064 nm)
	Pulse duration (9 ns), lens focal length (10 cm)
	Laser intensity (1.9–9.9×10^9 W/cm^2)
Collection optics	Located 10 cm from the focused spot
	Optical fiber cable placed at 45° angle
Optical spectrometer	Spectral scope (250–650 nm)
	CCD camera
Sample	Human teeth

Fig. 2 Predominated emission lines are produced by two different wavelengths (1064 and 532 nm)
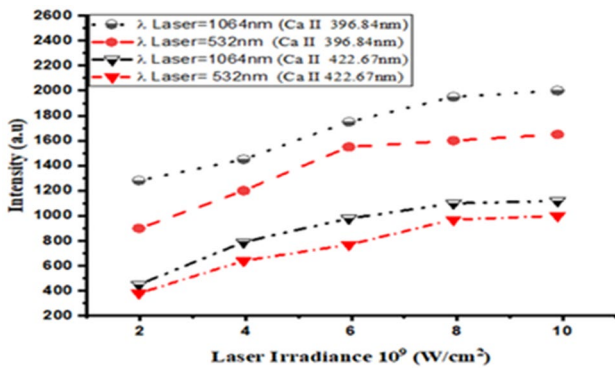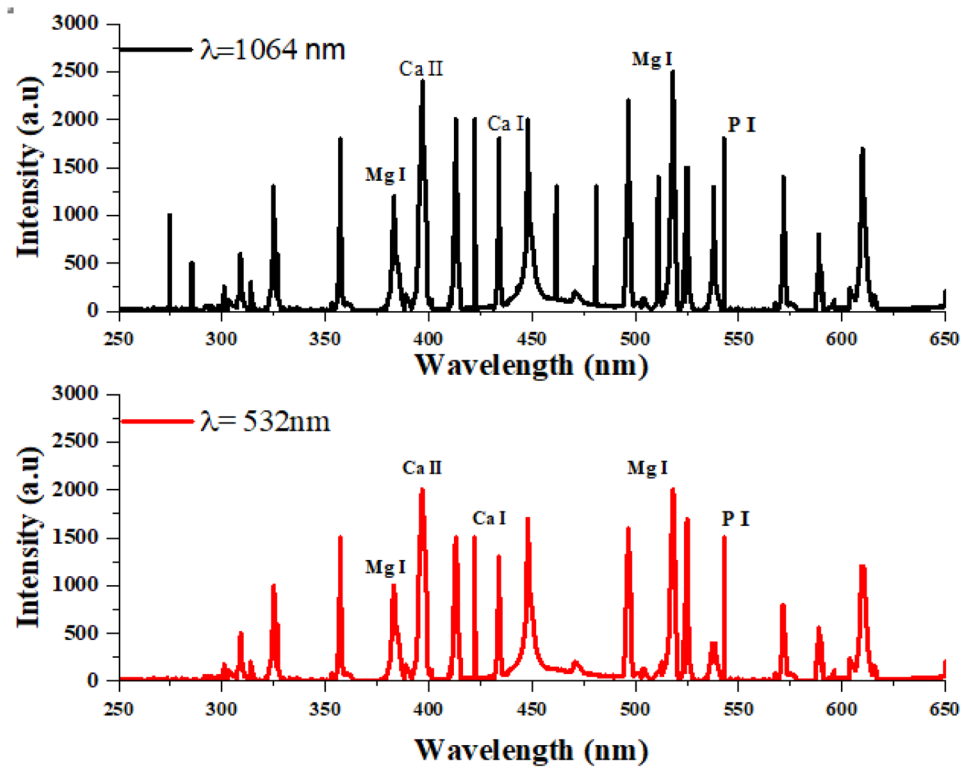

Fig. 3 Emission peak intensity for Ca II 396.84 nm (circles) and Ca II 422.67 nm (triangle) at 1064 and 532 nm

activities during plasma production. One of the acceptable methods for determining the electron temperature in the local thermodynamic equilibrium is the Boltzmann plot [15, 18], expressed as follows:

$$\ln\left(\frac{\lambda_{ij}I_{ij}}{g_iA_{ij}}\right) = -\frac{E_j}{k_B T_e} + \ln\frac{N(T)}{U(T)} \qquad (1)$$

where $\lambda_{ij}I_{ij}$, g_j, A_{ij}, and E_j are the wavelength, line intensity, statistical weight, transition probability, and excited level energy. $N(T)$ and $U(T)$ are the plasma number density and the partition function.

A graph in Fig. 4 is plotted concerning excitation energy E_j (in eV) and ln $(\lambda_{ij}I_{ij}/g_jA_{ij})$, T_e in kelvin is concluded from the slope $(1/k_B T)$ of the linear line. The excitation temperature was 10,549 K for 1064 nm and 10,179 K for 532 nm recorded at laser power density of 1.9×10^9 W/cm^2.

We show the variation of the electron temperature with the laser irradiances in Fig. 5, it was found that the T_e values increased with increasing laser irradiation. The electron temperature at wavelength of 1064 nm was higher than that recognized at 532 nm due to the change in optical absorption at longer wavelengths [19, 20].

Variation of electron number density

By using Saha–Boltzmann expression given by Eq. (2) [15], electron density N_e is established via the intensity ratio of two spectral lines of the same element (calcium) having different ionization stages

$$N_e = 6.04 * 10^{24}(T)^{3/2}\left(\frac{I\lambda}{gA}\right)_{ion}\left(\frac{gA}{I\lambda}\right)_{atom}$$
$$\times \exp\left[-\frac{(V^+ + E_{ion} - E_{atom})}{K_B T}\right] \qquad (2)$$

where I is the integrated emission intensity of the ion or atom, N_e is the electron density (cm^{-3}), gA is the product of
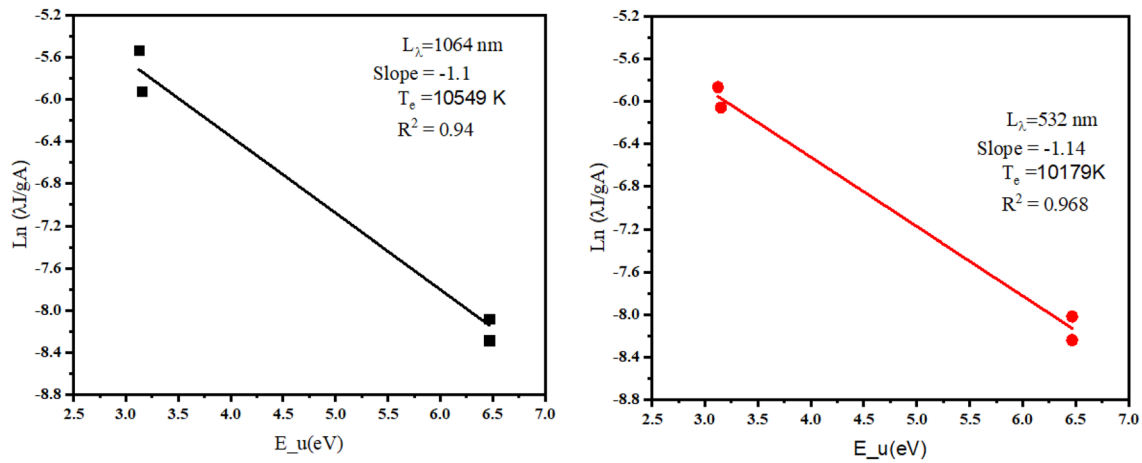
Fig. 4 Regular Boltzmann plot for Ca II emission lines at 1064 and 532 nm
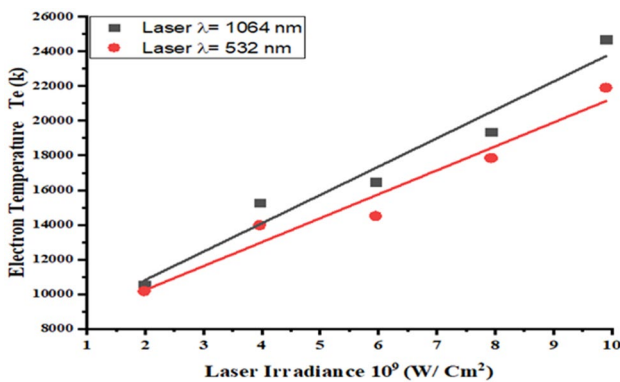

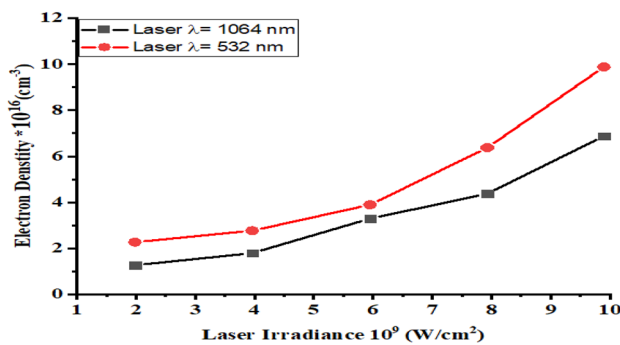**Fig. 5** Evaluation of the electron temperature at different laser irradiances

Fig. 6 Evaluation of N_e as a function of laser irradiance for wavelengths of 1064 (squares) and 532 nm (circles)

the statistical weight and Einstein coefficient for spontaneous emission of the upper level (s-1), λ is the wavelength (nm), E_{ion} is the excitation energy (upper level) of the ionic line (J), and E_{atom} is the excitation energy (upper level) of the atomic line (J).

Figure 6 displays the fluctuation in electron number densities as observed at both wavelengths at various Nd:YAG laser irradiances. There is a gradual increase in the values of N_e with the increasing of laser irradiance. Also, at the same pulse energy, the value of N_e formed at 532 nm is more than its corresponding value formed at 1064 nm. This was caused by increased multi-photon ionization and light matter coupling at shorter wavelengths [21].

Calculation of other plasma parameters

With the purpose of getting better understanding of plasma properties, other characteristic parameters such as Debye length (λ_D), number of particles in Debye sphere (N_D), and plasma frequency (ω_p) are obtained. The length of Debye is the distance at which an individual particle influences another charged particle carrying a reverse charge is inversely proportional to N_e and directly to square root of the electron temperature T_e, according to [22].

$$\lambda_D = \left(\frac{\varepsilon_0 k_B T_e}{N_e e^2} \right)^{0.5} \tag{3}$$

The variation of Debye length at various laser irradiation levels is displayed by Fig. 7. The calculated range of λ_D was $6.29–4.13 \times 10^{-8}$ cm for 1064 nm and $4.6–3.26 \times 10^{-8}$ cm for 532 nm. For both wavelengths, as more light being absorbed by the material, λ_D contracted as the laser energy increased. Since λ_D illustrates the shielding length, the self-focusing of laser beams will improve on condition that λ_D is less than the diameter of laser beam.

In addition, Debye number can be obtained from $N_D = \frac{4\pi}{3} \lambda_D^3 N_e$. Due to the direct relationship between N_D
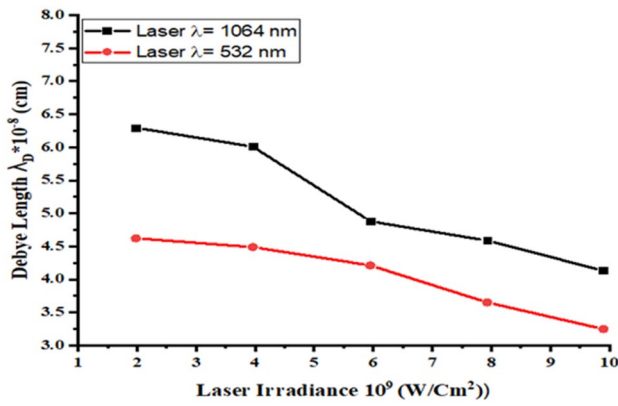
Fig. 7 Variation of λ_D for 1064 (squares) and 532 nm (circles) wavelengths at different laser irradiances
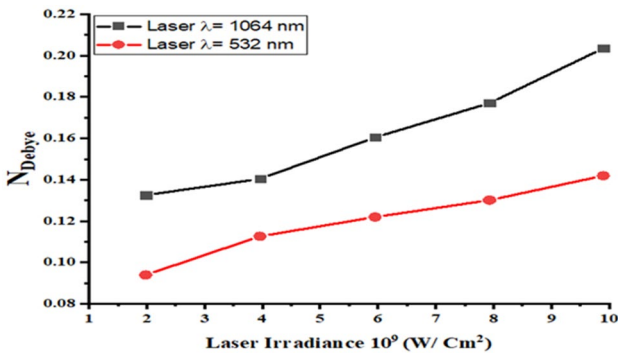

Fig. 8 Evaluation of Debye number for 1064 nm (squares) and 532 nm (circles) wavelengths at different laser irradiances

and λ_D, their reaction to variation of laser irritation will be identical. Figure 8 shows the variation of N_D at different laser irradiances, the calculated range of N_D was 0.13–0.2 for 1064 nm and 0.09–0.14 for 532 nm.

Moreover, plasma frequency (ω_p) was evaluated by [1, 23]:

$$\omega_p = 8.98 \times 10^3 \times N_e^{1/2}\ \text{Hz} \tag{4}$$

According to Eq. (4), plasma frequencies are directly proportional to $(N_e)^{0.5}$, and their results are reliable on electron density. Figure 9 shows plasma frequency (ω_p) at various laser irradiances. As higher laser irradiance produces relatively more plasma species, the values of ω_p improved with the increase in irradiance. Furthermore, in laser–plasma interaction, light may be transmitted, scattered, and /or absorbed. As soon as the frequency of the incident laser (ω_L) is higher than ω_p, laser light could
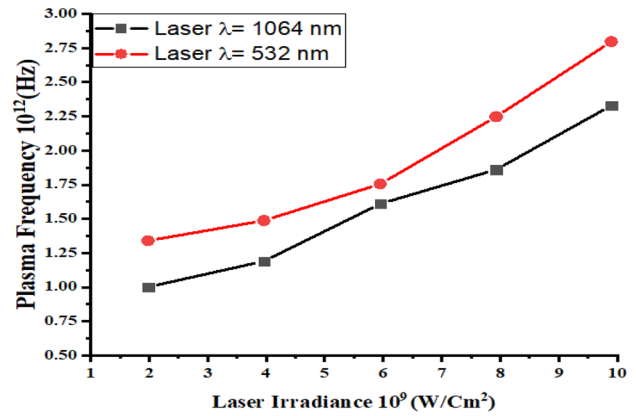

Fig. 9 Evaluation of plasma frequency for both 1064 (squares) and 532 nm (circles) at different laser irradiances

be reflected [22, 24], the maximum frequency of plasma calculated using Eq. (4) at laser irradiance of 9.9×10^9 w/cm^2 were 2.33, 2.79×10^{12} Hz for 1064 nm and 532 nm. Taking into account, the frequencies for Nd:YAG laser are equal to 2.8, 5.64×10^{14} Hz for 1064 nm and 532 nm, these two values are larger than the values of ω_p. Consequently, the losing energy by reflection is negligible.

Conclusion

The significant properties of plasma produced at the tooth surface were examined. Pulsed Nd:YAG laser with irradiance ranging from 1.9 to 9.9×10^9 W/cm^2. Optical emission analysis has been used to deduce several characteristic emission lines of Ca. The effect of laser irradiance and wavelength was evaluated, it was observed that teeth plasma parameters (electron temperature and number density) are remarkably enhanced at all laser irradiances, their maximum values are attributed to developing maximum ablation rate, plasma temperatures are highest in the case of $\lambda = 1064$ nm. Furthermore, similar behavior of increasing plasma frequency, Debye length, and number as a function of laser irradiance was also described.

References

1. A.N. Kadachi, M.A. Al-Eshaikh, Effect of optimum parameters setting on laser-induced breakdown spectroscopy. Spectrosc. Lett. **48**(6), 403–410 (2015)
2. J. Hoffman, T. Moscicki, Z. Szymanski, The effect of laser wavelength on heating of ablated carbon plume. Appl. Phys. A Mater. Sci. Process. **104**(3), 815–819 (2011)
3. I. Vlădoiu, M. Stafe, C. Neguţu, I.M. Popescu, "Nanopulsed ablation rate of metals dependence on the laser fluence and wavelength

in atmospheric air." UPB Sci. Bull. Ser. A Appl. Math. Phys. **70**(4), 119–126 (2008)

4. W. Luo, X. Zhao, S. Lv, H. Zhu, Measurements of egg shell plasma parameters using laser-induced breakdown spectroscopy. Pramana **85**(1), 105–114 (2015)

5. T. Hussain, M.A. Gondal, and M. Shamraiz, Determination of plasma temperature and electron density of iron in iron slag samples using laser induced breakdown spectroscopy.

6. H.T. Salloom, T.K. Hamad, F.H. Rajab, Laser-induced breakdown spectroscopy for determination of toxic metals in fertilizers: emphasis on Lead. Iraqi J. Sci. **63**(6), 2523–2531 (2022)

7. A.M. El Sherbini, A.A.S. Al Aamer, A.T. Hassan, T.M. El Sherbini, Measurements of plasma electron temperature utilizing magnesium lines appeared in laser produced aluminum plasma in air. Opt. Photonics J. **02**(04), 278–285 (2012)

8. S. Device, Quantitative analysis of cerium-gallium alloys using a hand-held laser induced breakdown spectroscopy device, (2019).

9. A. Syuhada Mangsor, Z. Haider Rizvi, K. Chaudhary, and M. Safwan Aziz, "Classification of alloys using laser induced breakdown spectroscopy with principle component analysis, J. Phys. Conf. Ser., 1027(1), (2018).

10. H. Sattar, H. Ran, W. Ding, M. Imran, M. Amir, H. Ding, An approach of stand-off measuring hardness of tungsten heavy alloys using LIBS. Appl. Phys. B Lasers Opt. **126**(1), 1–11 (2020)

11. H.T. Salloom, T.K. Hamad, A.H. Mohammed, Detection of harmful metal elements in rice using laser induced breakdown spectroscopy. J. Phys. Conf. Ser. **1**, 2021 (1818)

12. H. Salloom, T. Hamad, Investigation of compositional analysis and physical properties for Ni-Cr-Nb alloys using laser-induced breakdown spectroscopy. Opt. Appl. **51**(3), 429–444 (2021)

13. S. Hemeda, Laser induced breakdown spectroscopy and other analytical techniques applied on construction materials," 13(2), 103–119, (2013).

14. A. Kramida, Y. Ralchenko, J. Reader, and NIST ASD Team, NIST atomic spectra database lines form, *NIST Atomic Spectra Database (ver. 5.2) [Online]*, 2014. [Online]. Available: http://physics.nist.gov/asd.

15. T.K. Hamad, A.S. Jasim, and H.T. Salloom, Characterizing laser-induced plasma generated from MgO/PVA solid targets, Opt. Spectrosc., 127(1), (2019).

16. A.E. Hussein, P.K. Diwakar, S.S. Harilal, A. Hassanein, The role of laser wavelength on plasma generation and expansion of ablation plumes in air. J. Appl. Phys. **113**(14), 1–10 (2013)

17. M.A. Kasem, J.J. Gonzalez, R.E. Russo, M.A. Harith, Effect of the wavelength on laser induced breakdown spectrometric analysis of archaeological bone. Spectrochim. Acta - Part B At. Spectrosc. **101**, 26–31 (2014)

18. A. Safeen et al., Measurement of plasma parameters for copper using laser induced breakdown spectroscopy. Dig. J. Nanomater. Biostructures **14**(1), 29–35 (2019)

19. X. Bai et al., "Influence of ns-laser wavelength in laser-induced breakdown spectroscopy for discrimination of painting techniques. Spectrochim. Acta - Part B At. Spectrosc. **134**, 81–90 (2017)

20. M.A. Naeem, M. Iqbal, N. Amin, M. Musadiq, Y. Jamil, F. Cecil, Measurement of electron density and temperature of laser-induced copper plasma. Asian J. Chem. **25**(4), 2192–2198 (2013)

21. M. Hanif, M. Salik, Diagnostics of tin plasma produced by visible and IR nanosecond laser ablation. Contrib. Plasma Phys. **55**(4), 290–298 (2015)

22. N.M. Shaikh, S. Hafeez, B. Rashid, S. Mahmood, M.A. Baig, Optical emission studies of the mercury plasma generated by the fundamental, second and third harmonics of a Nd : YAG laser. J. Phys. D Appl. Phys. **39**(20), 4377–4385 (2006)

23. K. A. Aadim, Optical emission spectroscopic analysis of plasma parameters in tin–copper alloy co-sputtering system, Opt. Quantum Electron., 48(12), (2016).

24. M. Fikry, W. Tawfik, M.M. Omar, Investigation on the effects of laser parameters on the plasma profile of copper using picosecond laser induced plasma spectroscopy. Opt. Quantum Electron. **52**(249), 1–16 (2020)